AGU PUBLICATIONS

Geophysical Research Letters

RESEARCH LETTER
10.1002/2013GL059113

Key Points:
- NAM/NAO is marked by a meridional dipole in upper tropospheric clouds
- NAM/NAO-related cloud anomalies lead to marked cloud radiative forcing (CRF) anomalies
- The CRF anomalies act to shorten the timescale of the NAM/NAO-related temperature anomalies

Correspondence to:
Y. Li,
yingli@atmos.colostate.edu

Citation:
Li, Y., D. W. J. Thompson, Y. Huang, and M. Zhang (2014), Observed linkages between the northern annular mode/North Atlantic Oscillation, cloud incidence, and cloud radiative forcing, *Geophys. Res. Lett.*, *41*, 1681–1688, doi:10.1002/2013GL059113.

Received 28 JAN 2014
Accepted 30 JAN 2014
Accepted article online 6 FEB 2014
Published online 5 MAR 2014

Observed linkages between the northern annular mode/North Atlantic Oscillation, cloud incidence, and cloud radiative forcing

Ying Li[1], David W. J. Thompson[1], Yi Huang[2], and Minghong Zhang[2]

[1]Department of Atmospheric Science, Colorado State University, Fort Collins, Colorado, USA, [2]Department of Atmospheric and Oceanic Sciences, McGill University, Montreal, Quebec, Canada

Abstract The signature of the northern annular mode/North Atlantic Oscillation (NAM/NAO) in the vertical and horizontal distribution of tropospheric cloudiness is investigated in CloudSat and CALIPSO data from June 2006 to April 2011. During the Northern Hemisphere winter, the positive polarity of the NAM/NAO is marked by increases in zonally averaged cloud incidence north of ~60°N, decreases between ~25 and 50°N, and increases in the subtropics. The tripolar-like anomalies in cloud incidence associated with the NAM/NAO are largest over the North Atlantic Ocean basin/Middle East and are physically consistent with the NAM/NAO-related anomalies in vertical motion. Importantly, the NAM/NAO-related anomalies in tropospheric cloud incidence lead to significant top of atmosphere cloud radiative forcing anomalies that are comparable in amplitude to those associated with the NAM/NAO-related temperature anomalies. The results provide observational evidence that the most prominent pattern of Northern Hemisphere climate variability is significantly linked to variations in cloud radiative forcing. Implications for two-way feedback between extratropical dynamics and cloud radiative forcing are discussed.

1. Introduction

Clouds greatly impact the radiative budget of the Earth-atmosphere system. They cool the Earth by reflecting incoming shortwave radiation back to space but warm it by trapping outgoing longwave radiation [e.g., *Ramanathan et al.*, 1989; *Rossow and Lacis*, 1990; *Wielicki et al.*, 1995; *Stephens*, 2005; *Bony et al.*, 2006]. Since radiation fundamentally modifies the thermodynamic structure of the atmosphere, changes in cloud amount can also influence the large-scale atmospheric circulation [*Slingo and Slingo*, 1988; *Randall et al.*, 1989; *Stephens*, 2005]. Clouds at different altitudes and with varying optical depths affect the Earth's radiation budget in different ways, and detailed information of the global three-dimensional structure of clouds is key for determining the vertical distribution of radiative heating rates [*Wielicki and Parker*, 1992; *Chen et al.*, 2000; *Weare*, 2000]. Therefore, it is important to understand the signature of large-scale patterns of climate variability in cloud vertical structure and radiative forcing.

Previous observational and numerical studies have examined the effects of cloud-radiative forcing on the atmospheric circulation [*Slingo and Slingo*, 1988; *Randall et al.*, 1989; *Slingo and Slingo*, 1991]. The effects of clouds on the atmospheric circulation have been investigated over the tropics in association with the Madden-Julian Oscillation [e.g., *Slingo and Madden*, 1991; *Lee et al.*, 2001; *Bony and Emanuel*, 2001, 2005; *Zurovac-Jevtić et al.*, 2006]. Relatively little research effort has been placed on understanding the impact of cloud radiative effect on large-scale variability in the extratropical atmospheric circulation.

The northern annular mode/North Atlantic Oscillation (NAM/NAO) is the dominant pattern of climate variability in the Northern Hemisphere extratropical circulation [e.g., *Hurrell*, 1995; *Thompson and Wallace*, 2000; *Hurrell et al.*, 2003]. The NAM/NAO is associated not only with significant changes in the zonal wind but also in the mean meridional circulation and thus presumably the vertical structure of cloud incidence. The signature of the NAM/NAO in clouds has been studied in ship observations of low clouds [*Park and Leovy*, 2000] and in CloudSat data of cloud vertical distribution over the Arctic [*Devasthale et al.*, 2012]. The above studies demonstrate that the NAM/NAO has a robust regional signature in clouds, but they do not explore the attendant changes in cloud radiative forcing. *Previdi and Veron* [2007] examined the signature of the NAO in cloud cover and cloud radiative forcing over the high-latitude North Atlantic. However, their study focuses only on the northern high latitudes, and their cloud radiative forcing is estimated as the simple difference

between all-sky and clear-sky condition, which does not necessarily accurately quantify the cloud radiative effect [*Soden et al.*, 2008].

The objective of this study is to examine and interpret the signature of the NAM/NAO in the horizontal and vertical structures of cloud incidence and cloud radiative forcing using nearly 5 years of CloudSat/CALIPSO data. The data and methodology are described in section 2; the results are presented in section 3; and the implications of the results are discussed in section 4.

2. Data and Methodology

2.1. Data

We use the cloud fraction data obtained from the combined radar and lidar retrievals 2B-GEOPROF-LIDAR product (version P2R04) [*Mace et al.*, 2009]. The results are presented in terms of "cloud incidence", which provides a quantitative estimate of the likelihood of a cloud within a given volume sensed by the satellite [*Verlinden et al.*, 2011; *Li and Thompson*, 2013]. For example, a cloud incidence value of 50% indicates that a cloud was observed 50% of the time. We construct cloud incidence data with spatial resolution 2.5° (latitude) × 2.5° (longitude) × 240 m (vertical). The analyses here are based on ~5 years of CloudSat observations from June 2006 to April 2011.

Various fields are also derived from monthly mean output from the European Centre for Medium Range Weather Forecasts Re-Analysis-Interim (ERA-Interim) [*Simmons et al.*, 2007]. The ERA-Interim is used to calculate the surface temperature, atmospheric temperature, specific humidity, surface albedo, top of the atmosphere (TOA) radiation fluxes anomalies associated with the NAM/NAO. It is also used to supplement the satellite-derived cloud incidence. The reanalysis is available on a 1.5° × 1.5° horizontal mesh, at 37 pressure levels from 1979 to present. The forecast Interim products (e.g., radiative fluxes) are calculated using output at forecast steps of 6 and 12 h. We use ERA-Interim for the period of overlap with the CloudSat data (June 2006 through April 2011). Anomalies are computed by subtracting the annual cycle calculated for the period January 1979 to December 2011.

Monthly mean values of the NAM/NAO index are obtained from National Oceanic and Atmospheric Administration Climate Prediction Center (http://www.cpc.ncep.noaa.gov/products/precip/CWlink/daily_ao_index/ao.shtml) and are defined as the leading principal component of monthly mean 1000 hPa height during the period 1979–2000. The analysis is focused on the Northern Hemisphere cold season months October–March.

2.2. Decomposition of Radiation Anomalies Associated With the NAM/NAO

We apply the radiative kernel method [*Huang et al.*, 2007; *Soden et al.*, 2008; *Shell et al.*, 2008] to diagnose variations in TOA radiative fluxes associated with the NAM/NAO. The longwave radiative flux anomalies are decomposed into contributions from changes in surface and atmospheric temperature, atmospheric water vapor, and cloud; the shortwave radiative flux anomalies are decomposed into contributions from changes in surface albedo, atmospheric water vapor, and cloud.

Taking the longwave radiation anomalies as an example, the clear-sky and all-sky anomalies are decomposed as follows:

$$\Delta R^{\text{clear}} = \Delta R_T^{\text{clear}} + \Delta R_q^{\text{clear}} + Z^{\text{clear}}, \tag{1}$$

$$\Delta R^{\text{all}} = \Delta R_T^{\text{all}} + \Delta R_q^{\text{all}} + \Delta R_{\text{cloud}} + Z^{\text{all}}, \tag{2}$$

where ΔR denotes the TOA longwave radiation anomalies associated with the NAM/NAO and ΔR_T, ΔR_q, and ΔR_{cloud} represent contributions from change in surface and atmospheric temperature, atmospheric water vapor, and cloud, respectively. Z is the residual term, which provides a measure of the fidelity of the linear decomposition assumption.

The noncloud contributions are calculated as follows:

$$\Delta R_T = \frac{\partial R}{\partial T}\Delta T; \Delta R_q = \frac{\partial R}{\partial q}\Delta q \tag{3}$$

where $\frac{\partial R}{\partial T}$ and $\frac{\partial R}{\partial q}$ are the precalculated global radiative kernels based on the Geophysical Fluid Dynamics Laboratory general circulation model [*Soden et al.*, 2008] and ΔT and Δq correspond to regression anomalies

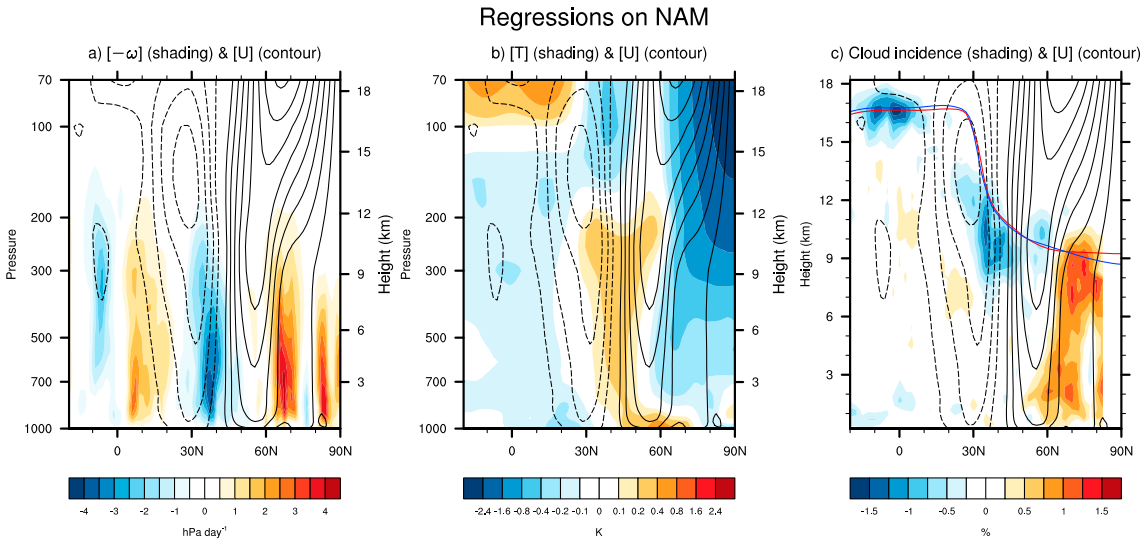

Figure 1. Regressions of zonal mean (a) pressure vertical motion (shading; ω has been multiplied by −1 so that positive values correspond to upward motion) and zonal wind (contour), (b) temperature (shading) and zonal wind (contour), and (c) cloud incidence (shading) and zonal wind (contour) onto standardized monthly mean values of the anomalous NAM/NAO index. Results are based on October–March data from June 2006 to April 2011. The seasonal cycle has been removed from the data. Units are K (temperature), hPa day^{-1} (pressure vertical motion), and % (cloud incidence). Contour interval of zonal wind is 0.5 m s^{-1} (dashed contours indicate negative values). The red and blue lines in Figure 1c indicate the climatological-mean tropopause height plus and minus the regression of tropopause height onto the standardized NAM/NAO index, respectively. Tropopause height is identified using the World Meteorological Organization lapse rate definition.

in surface and atmospheric temperature and atmospheric water vapor, respectively, associated with the NAM/NAO.

The cloud contribution is derived by combining equations (1) and (2)

$$\begin{aligned}\Delta R_{\text{cloud}} &= (\Delta R^{\text{all}} - \Delta R^{\text{clear}}) - (\Delta R_T^{\text{all}} - \Delta R_T^{\text{clear}}) - (\Delta R_q^{\text{all}} - \Delta R_q^{\text{clear}}) \\ &= (\Delta R^{\text{all}} - \Delta R^{\text{clear}}) - \left(\frac{\partial R^{all}}{\partial T} - \frac{\partial R^{\text{clear}}}{\partial T}\right)\Delta T - \left(\frac{\partial R^{\text{all}}}{\partial q} - \frac{\partial R^{\text{clear}}}{\partial q}\right)\Delta q. \end{aligned} \quad (4)$$

Note that the cloud radiative forcing (CRF) is defined as the difference between all-sky and clear- sky radiative anomalies (CRF $\equiv \Delta R^{\text{all}} - \Delta R^{\text{clear}}$) so that ΔR_{cloud} obtained by adjusting the CRF for the impacts of changes in T and q is often referred to as adjusted CRF [*Shell et al.*, 2008; *Soden et al.*, 2008].

3. Results

3.1. Zonally Averaged Circulation

Figures 1a and 1b review key aspects of the signature of the NAM/NAO in the zonal mean circulation. The contours in both panels correspond to the monthly mean zonal mean zonal wind anomalies regressed onto the NAM/NAO index. The shading in Figures 1a and 1b shows the corresponding anomalies in pressure vertical velocity (upward motion is positive) and atmospheric temperature, respectively.

As noted extensively in previous work [e.g., *Thompson and Wallace*, 2000; *Hurrell et al.*, 2003, and references therein], the positive polarity of the NAM/NAO is characterized by (1) a meridional dipole in the zonal mean zonal wind with centers of action located ~30°N and 55°N (Figure 1a) and (2) banded vertical motion (Figure 1a) and temperature (Figure 1b) anomalies in the troposphere that coincide roughly with the nodal lines in the changes in the zonal flow. The vertical motion anomalies are consistent with forcing by the anomalous momentum fluxes aloft and can be interpreted as driving (as opposed to responding to) the attendant changes in atmospheric temperature. The most pronounced temperature and vertical motion anomalies associated with the positive phase of the NAM/NAO include (1) warming at the tropical tropopause (consistent with a weakening of the stratospheric Brewer-Dobson circulation), (2) cooling and rising motion in the subtropical troposphere, (3) warming and sinking motion in the midlatitude troposphere, and (4) cooling and rising motion in the polar troposphere and stratosphere.

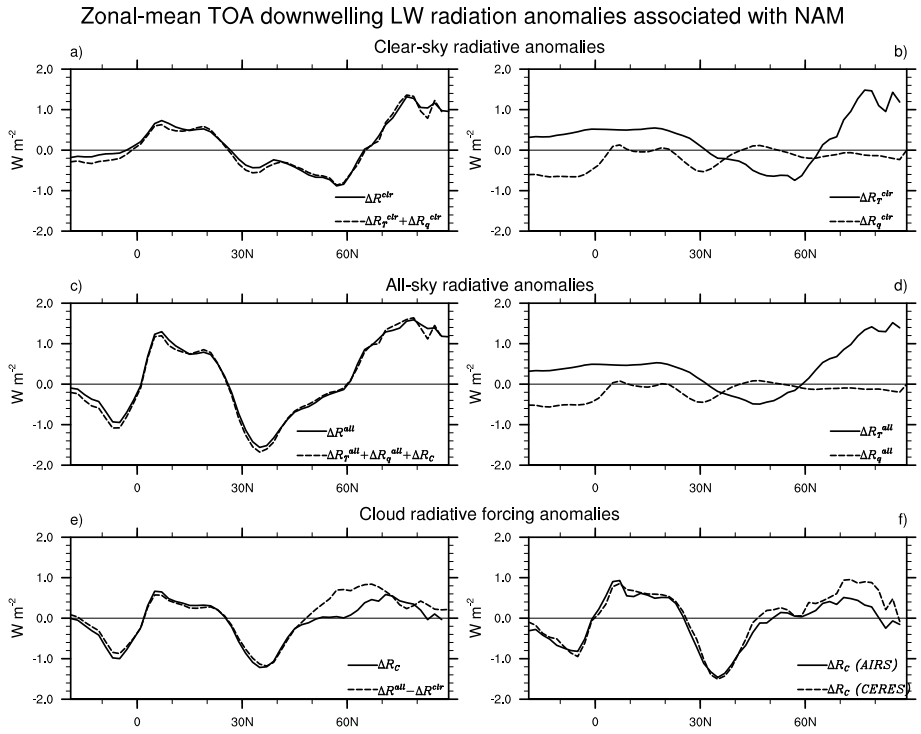

Figure 2. (a) Zonal mean TOA downwelling longwave clear-sky radiation anomalies associated with the NAM/NAO calculated directly from the ERA-Interim reanalysis (solid line) and derived from the sum of the contributions from various physical factors using the radiative kernel method (see equation (1); dashed line). (b) downwelling longwave radiation anomalies contributed from changes in temperature (solid line) and water vapor (dashed line). (c and d) As in Figures 2a and 2b, but for all-sky conditions. (e) Adjusted cloud radiative forcing (CRF) estimated using the radiative kernel method (solid line; see equation (4)), and CRF anomalies estimated as the simple difference between the all-sky and clear-sky radiative fluxes (dashed line). (f) Adjusted CRF based on AIRS (solid line) and CERES EBAF (dashed line) observations.

The shading in Figure 1c shows the corresponding changes in cloud incidence. The contours indicate the zonal wind and are reproduced from Figure 1b. The red and blue lines indicate the height of the tropopause during the positive (red) and negative (blue) polarities of the NAM/NAO. The positive polarity of the NAM/NAO is marked by a meridional dipole in upper tropospheric clouds with centers of action centered ~30–45°N and poleward of 60°N. The positive cloud anomalies poleward of 60°N extend throughout the troposphere, whereas the negative cloud anomalies at lower latitudes are confined to the upper troposphere. The lack of cloud anomalies in the subtropical lower troposphere may be due to the relatively low cloud amounts there; i.e., there are few clouds in the long-term mean to be perturbed by anomalies in the circulation.

For the most part, the largest anomalies in upper tropospheric cloud incidence coincide with the largest changes in vertical motion: downward anomalies in vertical motion at middle latitudes overlie decreases in cloud incidence; upward anomalies in vertical motion at high latitudes overlie increases in cloud incidence. The positive polarity of the NAM/NAO is also marked by decreases in cloud incidence near the tropical tropopause, consistent with the warming (shading in Figure 1a) and depression (red line in Figure 1c) of the tropical tropopause. The signature of the NAM/NAO in upper tropospheric cloud incidence is consistent with the linkages between cloud vertical structure and the large-scale meteorology demonstrated in *Li et al.* [2014]. The signature of the NAM/NAO in clouds at the tropical tropopause is consistent with the linkages between the Brewer-Dobson circulation and cloud incidence [*Li and Thompson*, 2013].

Figure 2 quantifies the zonal mean TOA longwave radiation anomalies associated with the NAM/NAO. Downward flux anomalies are defined as positive, such that positive anomalies correspond to a warming effect of clouds for the atmosphere-surface column. Figures 2a and 2c compare the longwave radiation anomalies associated with the NAM/NAO for clear-sky (Figure 2a) and all-sky (Figure 2c) conditions. Results indicated by the solid lines are calculated directly from the ERA-Interim reanalysis. Results indicated by

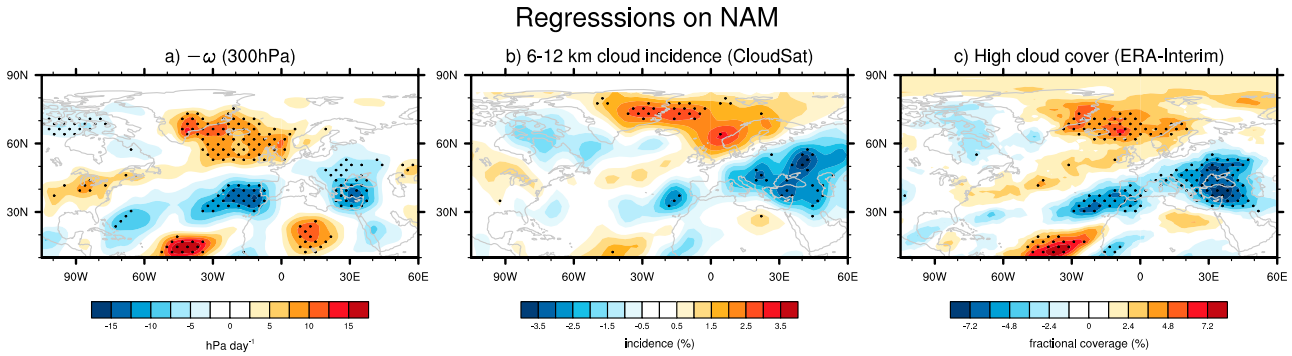

Figure 3. Regressions of monthly mean (a) pressure vertical motion (upward motion is positive) at 300 hPa, (b) cloud incidence averaged between 6 and 12 km based o CloudSat/CALIPSO data set, and (c) high-cloud fractional coverage based on ERA-Interim reanalysis onto standardized monthly mean values of the anomalous NAM/NAO index. Stippling indicates results that exceed 95% confidence level based on a two-tailed test of the *t* statistic, with the effective degrees of freedom computed given in *Bretherton et al.* [1999, equation (31)]. The results in Figures 3a and 3b have been smoothed with a National Center for Atmospheric Research Command Language built-in 9-point smoothing function for the purpose of display only.

the dashed lines are calculated as the sum of the contributions from temperature and water vapor (and clouds) using the radiative kernel method. The very close agreement between the solid and dashed lines in Figures 2a and 2c indicates that the residual terms in equations (1) and (2) are very small and thus that the linear decomposition of TOA radiation anomalies by the kernel method is robust. Figures 2b and 2d show the associated decomposition of the anomalies in longwave radiation due to the changes in temperature and water vapor under both clear sky (Figure 2b) and all sky (Figure 2d) conditions. The noncloud contributions to the net changes in longwave forcing are dominated by the changes in surface and atmospheric temperature (solid lines in Figures 2b and 2d).

Figure 2e shows the changes in longwave CRF (dashed) and adjusted longwave CRF (solid) associated with variability in the NAM/NAO. Both results indicate (1) longwave warming due to clouds north of ~60°N, where the NAM/NAO is associated with increases in cloud incidence and (2) longwave cooling due to clouds between ~25 and 50°N, where the NAM/NAO is associated with decreases in cloud incidence. The difference between the two longwave estimates within the latitude band ~50–70°N is centered over northern Eurasia (not shown), where the large surface warming associated with the NAM/NAO is accompanied by strong cooling in the troposphere, and thus a large increase in the temperature lapse rate. As noted in *Huang and Ramaswamy* [2009], such a large change in the lapse rate may be mistaken for a cloud radiative effect in simple differences between all-sky and clear-sky radiation.

We reproduced the analyses in Figure 2 based on TOA longwave radiative fluxes from Clouds and the Earth's Radiant Energy System (CERES) Energy Balanced and Filled (EBAF) Ed2.6r data product [*Loeb et al.*, 2009] and Atmospheric Infrared Sounder (AIRS) observations [*Chahine et al.*, 2006]. The meridional structure of the adjusted CRF anomalies based on both observational data sources (Figure 2f) are very similar to those derived from ERA-Interim (solid line in Figure 2e), albeit CERES has somewhat larger amplitude north of 70°N. Due to the strong similarity between results derived from both remotely sensed products and ERA-Interim, we will use the ERA-Interim reanalysis to estimate the radiative fluxes in the following sets of results.

3.2. North Atlantic Sector

Figure 3 shows three different fields regressed onto the NAM/NAO index over the North Atlantic sector: upper tropospheric (300 hPa) vertical motion from ERA-Interim (Figure 3a), upper tropospheric cloud incidence (averaged 6–12 km) from the CloudSat data set (Figure 3b); and high-level (above ~450 hPa) cloud cover from ERA-Interim (Figure 3c).

Variations in the NAM/NAO are marked by a range of cloud incidence anomalies over the North Atlantic sector. Poleward of ~55°N, the positive polarity of the NAM/NAO is marked by increases in upper tropospheric cloud incidence to the east of Greenland juxtaposed against much weaker decreases to the west (Figure 3b) [see also *Previdi and Veron*, 2007; *Devasthale et al.*, 2012]. At middle latitudes, the positive polarity of the NAM/NAO is associated with decreases in upper tropospheric cloud incidence that extend from the west of Gibraltar into eastern Europe. At subtropical latitudes, it is marked by weak increases in upper tropospheric

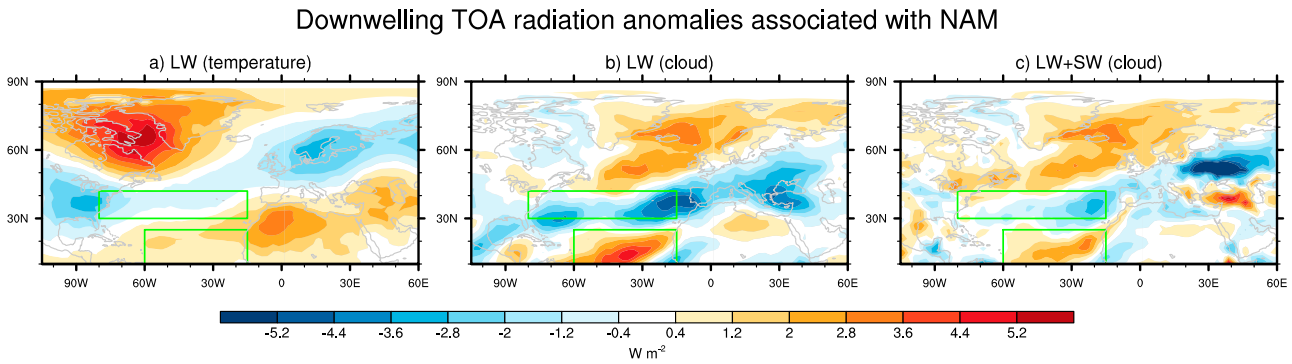

Figure 4. TOA downwelling radiation anomalies associated with the NAM/NAO contributed from (a) temperature (longwave), (b) cloud (longwave), and (c) cloud (longwave + shortwave). Green boxes indicate example regions where the radiation forcing anomalies due to the changes in temperature and clouds coincide with each other (see text for detail).

cloud incidence over the northern tropical Atlantic. The anomalies in cloud incidence over the eastern North Atlantic correspond to a poleward shift in the Northern Hemisphere midlatitude jet and are consistent with the pattern of the NAM/NAO in precipitation [e.g., *Hurrell*, 1995].

The significance of the cloud incidence results in Figure 3b is limited by the short CloudSat record. Nevertheless, it is worth noting that the changes in upper tropospheric cloud incidence indicated by CloudSat are reproducible in the ERA-Interim reanalysis (compare Figures 3b and 3c), and they are qualitatively consistent with the attendant changes in anomalous vertical velocity (compare Figures 3a and 3b).

Figure 4 shows the geographical distribution of the TOA radiation anomalies associated with the NAM/NAO. Since the contribution of water vapor to the NAM/NAO-related longwave radiation anomalies is small (see Figure 2d), we show only the contributions from temperature and clouds. The large contributions of the TOA longwave radiation anomalies due to changes in surface and atmospheric temperature are found over the continental areas (Figure 4a) and include (1) longwave cooling over southeastern U.S. and northern Eurasia (where the NAM/NAO induces surface warming) and (2) longwave warming over eastern Canada/Greenland and southwestern Asia/Northern Africa (where the NAM/NAO induces surface cooling). Both sets of anomalies are consistent with the negative Planck and lapse rate feedback.

As is the case for the zonal mean (Figure 2), the contribution of clouds to the NAM/NAO-related TOA longwave radiation anomalies over the Atlantic sector is comparable in amplitude to those due to temperature. The longwave cooling due to clouds peaks in a region extending eastward from the east coast of the U.S. to eastern Europe (Figure 4b) and is coincident with the decreases in high cloud incidence found over those locations (Figures 3b and 3c). The longwave warming due to clouds peaks over the subtropical North Atlantic and the subpolar North Atlantic (Figure 4b) and is coincident with the increases in high cloud incidence found over those regions (Figures 3b and 3c). The spatial consistency between the longwave adjusted CRF and the anomalous high cloud incidence from two independent data sets further corroborates the robustness of our estimate of variations in cloud radiative forcing due to variability in the NAM/NAO.

We also assessed the attendant changes in TOA cloud shortwave radiative forcing as adjusted to account for the impact of water vapor and surface albedo. The results of total adjusted CRF are shown in Figure 4c. The shortwave adjusted CRF is negligible over high latitudes where the incident solar radiation is very weak during winter. Over the North Atlantic middle/low latitudes, the shortwave adjusted CRF is still a factor of 2–3 smaller in magnitude than that due to the longwave forcing. Thus, the total adjusted CRF associated with the NAM/NAO is dominated by the longwave component.

4. Concluding Remarks

We have explored the signature of the NAM/NAO in the vertical and horizontal distribution of clouds and adjusted cloud radiative forcing (CRF) in both CloudSat/CALIPSO data and ERA-Interim reanalysis. The positive polarity of the NAM/NAO is marked by coherent and robust changes in cloud incidence that largely mirror its attendant changes in vertical motion. The changes in cloud incidence associated with the NAM/NAO, in turn, lead to marked anomalies in adjusted CRF. Over the North Atlantic, the anomalies in

adjusted CRF are due primarily to changes in the fluxes of longwave radiation and are comparable in amplitude to the changes in radiative flux due to the NAM/NAO-related temperature anomalies. The primary cloud incidence and adjusted CRF anomalies associated with the NAM/NAO were found to be reproducible in independent data sources and using different analysis techniques.

In the absence of land-sea contrasts, the adjusted CRF anomalies associated with annular variability might be expected to shorten the timescale of the attendant temperature anomalies. For example, regions of large-scale ascent and cooling are marked by increases in cloud incidence, and the resulting positive anomalies in longwave adjusted CRF should act to shorten the timescale of the negative atmospheric temperature anomalies (e.g., north of 60°N in Figures 1 and 2e).

In the presence of large land-sea contrasts, the temperature anomalies associated with the NAM/NAO are dominated by horizontal temperature advection (as opposed to vertical motion). Over the high latitudes of the North Atlantic, the cloud and temperature radiative forcing anomalies associated with the NAM/NAO do not clearly coincide with each other (compare Figures 4a and 4c). Over the middle/low latitudes of the North Atlantic, the TOA adjusted CRF anomalies generally reinforce those due to the changes in temperature (e.g., see green boxes of Figure 4). Hence, over the middle/low latitudes of the North Atlantic, the adjusted CRF should act to shorten the timescale of the middle/low latitude temperature anomalies associated with the NAM/NAO. The importance of cloud and temperature radiative feedback in determining the timescale of large-scale atmospheric phenomena will be examined in a companion study.

Finally, we note that the net hemispheric-mean cloud-radiative effect associated with the NAM/NAO is a warming effect of 0.26 (longwave) − 0.04 (shortwave) = +0.22 W m^{-2}. For comparison, *Grise et al.* [2013] argue that the hemispheric-mean cloud radiative anomalies induced by (1) the Antarctic ozone hole is ~0.25 W m^{-2} and (2) the Southern Annular Mode (SAM) is ~0.18 W m^{-2}. That said, it should be born in mind that their results are based on very different seasonal averages (the cloud radiative anomaly associated with SAM is based on austral summer when the shortwave forcing dominates the long wave forcing; the cloud radiative anomaly associated with the ozone hole is based on the annual mean). The differences in seasonal averages, cloud data, periods of analysis, and radiative kernel methodologies between our study and *Grise et al.* [2013] likely have a notable effect on the magnitude of the estimated hemisphere-mean radiation values. Future work is needed to further verify and understand the hemispheric-mean cloud radiative feedback associated with NAM.

Acknowledgments

We thank Graeme L. Stephens, Andrew Dessler, Jian Lu, and Kevin Grise for helpful discussion of the results. We would also like to thank Yen-Ting Hwang and an anonymous reviewer for constructive and insightful comments on the manuscript. YL was funded by CloudSAT via NASA JPL and the NSF Climate Dynamics program. DWJT is funded by the NSF Climate Dynamics program.

The Editor thanks Yen-Ting Hwang and an anonymous reviewer for their assistance in evaluating this paper.

References

Bony, S., and K. A. Emanuel (2001), A parameterization of the cloudiness associated with cumulus convection: Evaluation using TOGA COARE data, *J. Atmos. Sci.*, *58*, 3158–3183.

Bony, S., and K. A. Emanuel (2005), On the role of moist processes in tropical intraseasonal variability: Cloud-radiation and moisture-convection feedbacks, *J. Atmos. Sci.*, *62*, 2770–2789.

Bony, S., et al. (2006), How well do we understand and evaluate climate change feedback processes?, *J. Clim.*, *19*, 3445–3482.

Bretherton, C. S., M. Widmann, V. P. Dymnikov, J. M. Wallace, and I. Bladé (1999), The effective number of spatial degrees of freedom of a time-varying field, *J. Clim.*, *12*, 1990–2009.

Chahine, M., et al. (2006), Improving weather forecasting and providing new data on greenhouse gases, *Bull. Am. Meteorol. Soc.*, *87*, 911–926.

Chen, T., Y. C. Zhang, and W. B. Rossow (2000), Sensitivity of atmospheric radiative heating rate profiles to variations of cloud layer overlap, *J. Clim.*, *13*, 2941–2959.

Devasthale, A., M. C. M. Tjernström, M. A. Thomas, B. H. Kahn, and E. J. Fetzer (2012), Influence of the Arctic Oscillation on the vertical distribution of clouds as observed by the A-Train constellation of satellites, *Atmos. Chem. Phys.*, *12*, 10,535–10,544.

Grise, K. M., L. M. Polvani, G. Tselioudis, Y. Wu, and M. D. Zelinka (2013), The ozone hole indirect effect: Cloud-radiative anomalies accompanying the poleward shift of the eddy-driven jet in the Southern Hemisphere, *Geophys. Res. Lett.*, *40*, 3688–3692, doi:10.1002/grl.50675.

Huang, Y., and V. Ramaswamy (2009), Evolution and trend of the outgoing longwave radiation spectrum, *J. Clim.*, *22*, 4637–4651, doi:10.1175/2009JCLI2874.1.

Huang, Y., V. Ramaswamy, and B. Soden (2007), An investigation of the sensitivity of the clear-sky outgoing longwave radiation to atmospheric temperature and water vapor, *J. Geophys. Res.*, *112*, D05104, doi:10.1029/2005JD006906.

Hurrell, J., Y. Kushnir, M. Visbeck, and G. Ottersen (2003), An overview of the North Atlantic Oscillation, in *The North Atlantic Oscillation: Climatic Significance and Environmental Impact, Geophys. Monogr. Ser.*, vol. 134, edited by J. W. Hurrell et al., pp. 1–35, AGU, Washington, D. C., doi:10.1029/134GM01.

Hurrell, J. W. (1995), Decadal trends in the North Atlantic Oscillation regional temperatures and precipitation, *Science*, *269*, 676–679.

Lee, M.-I., I.-S. Kang, J.-K. Kim, and B. E. Mapes (2001), Influence of cloud-radiation interaction on simulating tropical intraseasonal oscillation with an atmospheric general circulation model, *J. Geophys. Res.*, *106*, 14,219–14,233.

Li, Y., and D. W. J. Thompson (2013), The signature of the stratospheric Brewer-Dobson circulation in tropospheric clouds, *J. Geophys. Res. Atmos.*, *118*, 3486–3494, doi:10.1002/jgrd.50339.

Li, Y., D. W. J. Thompson, G. L. Stephens, and S. Bony (2014), A global survey of the instantaneous linkages between cloud vertical structure and large-scale climate, *J. Geophys. Res.*, doi:10.1002/2013JD020669, in press.

Loeb, N. G., B. A. Wielicki, D. R. Doelling, G. L. Smith, D. F. Keyes, S. Kato, N. Manlo-Smith, and T. Wong (2009), Toward optimal closure of the Earths top-of-atmosphere radiation budget, *J. Clim*, *22*, 748–766.

Mace, G. G., Q. Zhang, M. Vaughn, R. Marchand, G. Stephens, C. Trepte, and D. Winker (2009), A description of hydrometeor layer occurrence statistics derived from the first year of merged CloudSat and CALIPSO data, *J. Geophys. Res.*, *114*, D00A26, doi:10.1029/2007JD009755.

Park, S., and C. B. Leovy (2000), Winter North Atlantic low cloud anomalies associated with the northern hemisphere annular mode, *Geophys. Res. Lett.*, *27*, 3357–3360.

Previdi, M., and D. E. Veron (2007), North Atlantic cloud cover response to the North Atlantic oscillation and relationship to surface temperature changes, *J. Geophys. Res.*, *112*, D07104, doi:10.1029/2006JD007516.

Ramanathan, V., R. D. Cess, E. F. Harrison, P. Minnis, B. R. Barkstrom, E. Ahmad, and D. Hartmann (1989), Cloud-radiative forcing and climate: Results from the Earth radiation budget experiment, *Science*, *243*, 57–63.

Randall, D. A., Harshvardhan, D. A. Dazlich, and T. G. Corsett (1989), Interactions among radiation, convection, and large-scale dynamics in a general circulation model, *J. Atmos. Sci.*, *46*, 1943–1970.

Rossow, W. B., and A. A. Lacis (1990), Global, seasonal cloud variations from satellite radiance measurements. Part II. Cloud properties and radiative effects, *J. Clim.*, *3*, 1204–1253.

Shell, K. M., J. T. Kiehl, and C. A. Shields (2008), Using the radiative kernel technique to calculate climate feedbacks in NCAR's Community Atmospheric Model, *J. Clim.*, *21*, 2269–2282.

Simmons, A., S. Uppala, D. Dee, and S. Kobayashi (2007), ERA-Interim: New ECMWF reanalysis products from 1989 onwards, *ECMWF Newsletter*, *110*, 25–35, ECMWF, Reading, U. K.

Slingo, A., and R. A. Madden (1991), Characteristics of the tropical intraseasonal oscillation in the NCAR community climate model, *Q. J. R. Meteorolog. Soc.*, *117*, 1129–1169.

Slingo, A., and J. M. Slingo (1988), The response of a general circulation model to cloud longwave radiative forcing. I: Introduction and initial experiments, *Q. J. R. Meteorolog. Soc.*, *114*, 1027–1062.

Slingo, J. M., and A. Slingo (1991), The response of a general circulation model to cloud longwave radiative forcing. II: Further studies, *Q. J. R. Meteorolog. Soc.*, *117*, 333–364.

Soden, B. J., I. M. Held, R. Colman, K. M. Shell, J. T. Kiehl, and C. A. Shield (2008), Quantifying climate feedbacks using radiative kernels, *J. Clim.*, *21*, 3504–3520.

Stephens, G. L. (2005), feedbacks in the climate system: A critical review, *J. Clim.*, *18*, 237–273.

Thompson, D. W. J., and J. M. Wallace (2000), Annular modes in the extratropical circulation. Part I: Month-tomonth variability, *J. Clim.*, *13*, 1000–1016.

Verlinden, K. L., D. W. J. Thompson, and G. L. Stephens (2011), The three-dimensional distribution of clouds over the Southern Hemisphere high latitudes, *J. Clim.*, *24*, 5799–5811.

Weare, B. C. (2000), Insights into the importance of cloud vertical structure in climate, *Clim. Dyn.*, *27*, 907–910.

Wielicki, B. A., and L. Parker (1992), On the determination of cloud cover from satellite sensors: The effect of sensor spatial resolution, *J. Geophys. Res.*, *97*, 12,799–12,823.

Wielicki, B. A., E. F. Harrison, R. D. Cess, M. D. King, and D. A. Randall (1995), Mission to planet Earth: Role of clouds and radiation in climate, *Bull. Am. Meteorol. Soc.*, *76*, 2125–2153.

Zurovac-Jevtić, D., S. Bony, and K. Emanuel (2006), On the role of clouds and moisture in tropical waves: A two-dimensional model study, *J. Atmos. Sci.*, *63*, 2140–2154.